Mn Valence, Magnetic, and Electrical Properties of $LaMnO_{3+\delta}$ Nanofibers by Electrospinning

Xianfeng Zhou,[†] Jiang Xue,[‡] Defeng Zhou,[§] Zhongli Wang,[†] Yijia Bai,[†] Xiaojie Wu,[†] Xiaojuan Liu,[‡] and Jian Meng*[,†]

State Key Laboratory of Rare Earth Resource Utilization, Changchun Institute of Applied Chemistry, Chinese Academy of Sciences, Changchun 130022, China, School of Materials Science and Engineering, Changchun University of Science and Technology, Changchun 130022, China, and School of Biological Engineering, Changchun University of Technology, Changchun 130012, China

ABSTRACT $LaMnO_{3+\delta}$ nanofibers have been prepared by electrospinning. The nearly 70% of Mn atoms is Mn^{4+}, which is much higher than that in the nanoparticles. The average grain size of our fibers is approximately 20 nm, which is the critical size producing the nanoscale effect. The nanofibers exhibit a very broad magnetic transition with $T_c \approx 255$ K, and the T_c onset is around 310 K. The blocking temperature T_B is 180 K. The sample shows weak ferromagnetic property above the T_B and below T_c and superparamagnetic property near the T_c onset. The resistivity measurements show a metal−insulator transition near 210 K and an upturn at about 45 K.

KEYWORDS: $LaMnO_{3+\delta}$ • nanofibers • Mn valence • magnetic property • electrical propery

$LaMnO_3$ and related compounds have attracted much attention due to their abundant physical properties such as Jahn−Teller effect, metal−insulator transition, colossal magnetoresistance effect and their potential applications in magneto-electronic devices, magneto-data storage (1−3). These properties are closely related to the interactions among charge, orbital, spin, lattice and magnetic degrees of freedom. Through cationic replacement in the A-type antiferromagnetic and insulating compound $LaMnO_3$, the $La_{1-x}A_xMnO_3$ Manganite transforms into a doped mixed-valence $Mn^{3+}-Mn^{4+}$ phase that is ferromagnetic and displays a metal−insulator transition in the vicinity of the T_c. The spin dynamics and electronic transport are conventionally interpreted in terms of the Zener double-exchange (DE) mechanism (4). The $Mn^{3+}-Mn^{4+}$ mixed-valence state can also be obtained by altering the chemical stoichiometry, as for self- or vacancy-doped samples with the general formula $La_{1-x}Mn_{1-y}O_{3+\delta}$. In these compounds, variations of x, y, and δ can modify the $Mn^{3+}-Mn^{4+}$ ratio, which is beneficial for activating the DE interaction. This enhances the ferromagnetic coupling and gives rise to the CMR effect as in the case of the substituted compounds (5−7).

It is well-known that one-dimensional ceramic nanoscales such as fibers, wires, and rods has received great interest owing to their potential applications in many technologically important areas such as electronics, photonics, and magnetics (8). In particular, magnetic nanostructures materials, because of the physics they involve and their potential technological applications, have been investigated widely in the past decade. Electrospinning represents a straightforward and versatile way for generating fibers with diameters ranging from tens of nanometers to several micrometers. This technique has been fabricated a large number of ultrafine fibers or nanofibers from a variety of materials, such as polymers, composites, and ceramics (9). The ceramic nanofibers synthesized via electrospinning were reported first in 2002 (10); Since then, this technique has been used to prepare a series of ceramic nanofibers that include, for example, Nb_2O_5, $LiFePO_4$ and $CoFe_2O_4$, etc. (11−13).

In recent years, many research groups have investigated the magnetic and transport properties of $LaMnO_{3+\delta}$ nanocrystalline or nanopowders (5−7, 14), but fewer studies on the $LaMnO_{3+\delta}$ nanofibers and their physical properties have been reported (15, 16). In this letter, electrospinning and sol−gel processing was combined to prepare $LaMnO_{3+\delta}$ nanofibers, and the valence state of the Mn ions, magnetic and electrical properties of $LaMnO_{3+\delta}$ nanofibers was investigated.

The preparation of $LaMnO_{3+\delta}$ nanofibers is similar to our previous publication (15); 5.145 g of $La(CH_3COO)_3 \cdot 1.5H_2O$ (Alfa Aesar) and 3.675 g of $Mn(CH_3COO)_2 \cdot 4H_2O$ (Alfa Aesar) were dissolved in 30 mL of deionized water. The precursor solution was stirred for 5 h, and then put into 30 mL of an aqueous PVA (ACROS ORGANICS, $M_w \approx 88\,000$) solution of 10 wt % and stirred for 30 h. The mixture was loaded into a plastic syringe. A piece of flat aluminum foil was placed ~18 cm below the tip of the needle to collect the nanofibers. Nonwoven mat structure hybrid fibers were fabricated by

* Corresponding author. Tel: +86-431-85262030. Fax: +86-431-85698041. E-mail: jmeng@ciac.jl.cn.

Received for review May 30, 2010 and accepted September 9, 2010

[†] Chinese Academy of Sciences.

[‡] Changchun University of Science and Technology.

[§] Changchun University of Technology.

DOI: 10.1021/am1004738

applied electric voltage of 16 kV. Finally, the as-prepared fibers were calcined at 400 °C for 2 h in order to remove PVA and volatile components, and then calcined the fibers in air at 600 °C for 2 h to obtain $LaMnO_{3+\delta}$ nanofibers. The scanning electron microscopy (SEM) images were recorded by JEOL JSM-6700F field-emission electron microscope. The transmission electron microscopy (TEM) measurement was performed using a JEM-2000EX instrument. The X-ray diffraction (XRD) pattern was obtained from Rigaku D/max-2500 X-ray diffractometer using Cu K_α radiation. The sample was mixed with KBr and pressed into pellet for Fourier transformed infrared (FT-IR) analysis on EQUINOX 55 spectrometer between 400 and 1200 cm^{-1}. The X-ray photoelectron spectroscopy (XPS) measurements were performed with ESCALAB-250 using an Al X-ray source emitting at 1486.6 eV. Magnetic properties were measured by superconducting quantum interference device (SQUID, Quantum Design MPMS-XL). Electronic properties were measured in a physical properties measurement system (PPMS, Quantum Design PPMS-9T).

The morphology and structure of the nanofibers is similar to our previous study (15). The results of SEM photographs show that the as-prepared hybrid fibers are smooth and their diameters range from 100 to 200 nm (Figure 1a). After calcinated at 600 °C, the fibers surface shrank and the diameters of nanofibers decreased and ranged from 50 to 100 nm (Figure 1b). The TEM image with corresponding electron diffractions (ED) of the $LaMnO_3$ nanofibers is shown in Figure 1c. The result verified that the average size of $LaMnO_3$ grains is approximately 20 nm in diameter. The ED of $LaMnO_3$ nanofibers showed the central halo and faint diffused rings, which revealed that it is essentially polycrystalline structure.

The XRD pattern is shown in Figure 2a. The results manifested that the final products completely crystallized into the cubic $LaMnO_3$ phase (space group $Pm\bar{3}m$ (221), JCPDS Card no. 75−0440). The average diameter of crystal grains calculated using the Scherrer formula is approximately 19 nm. The FT-IR spectrum of the $LaMnO_3$ nanofibers is shown in Figure 2b. The result shows that there is only one strong peak located at 601 cm^{-1} related to the stretching mode ν_3 of the MnO_6 octahedra with O_h^6 symmetry in the $LaMnO_3$ (17), and the vibrational modes for various manganese oxides were not found in the FT-IR spectrum (18). Therefore, the final nanofibers are pure $LaMnO_3$ based on the results of XRD and FT-IR.

The Mn^{3+}−Mn^{4+} ratio, or the valence of Mn, was checked by XPS. Figure 3a and Figure 3b show Mn 2p and Mn 3s XP spectra of the nanofibers sample. The 2p spectrum exhibits two broad lines with maxima at 641.9 and 653.5 eV for Mn $2p_{3/2}$ and Mn $2p_{1/2}$ emission, respectively. The binding energy of the Mn $2P_{3/2}$ peak is usually used to study the Mn valence state in manganites (5). It is known from the studies of lanthanum manganites that the binding energy of Mn^{3+} is close to 641.2 eV, whereas that of Mn^{4+} to 642.5 eV, and peak fitting on the Mn $2p_{3/2}$ of our sample, as shown in the inset of Figure 3a, was carried out using the XPSPEAK 3.01

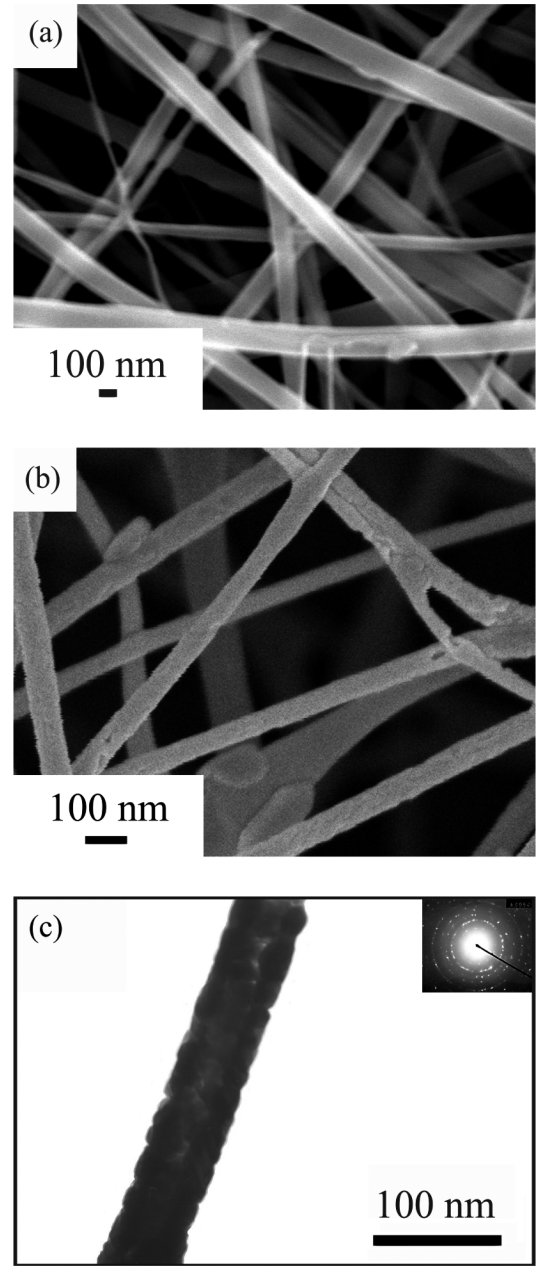

FIGURE 1. SEM images of (a) as-prepared hybrid fibers and (b) $LaMnO_{3+\delta}$ nanofibers, and (c) TEM image with corresponding ED of $LaMnO_{3+\delta}$ samples.

software. The result shows that the Mn oxidation state of our final fibers is somewhere between +3 and +4. The content of Mn^{4+} is estimated to be 72% for the nanofibers. Alternatively, the Mn valence ν_{Mn} can be obtained from the exchange splitting of the manganese 3s spectrum by employing the linear equation: $\nu_{Mn} = 9.67 - 1.27\Delta E_{3s}$/eV, where the linear relationship between ν_{Mn} and ΔE_{3s} is derived for the valence range between +3 and +4 from XPS investigations of different mixed-valence manganites and of binary Mn oxides, respectively (19, 20). The ΔE_{3s} is found to be 4.70 eV in Figure 3b after fitting, so the manganese valence is equal to +3.72 or there are approximately 70% Mn^{4+} ions in the $LaMnO_3$ samples, which is much higher than that in the nanoparticles (5, 6). Therefore, our sample exhibits significant oxygen off-stoichiom-

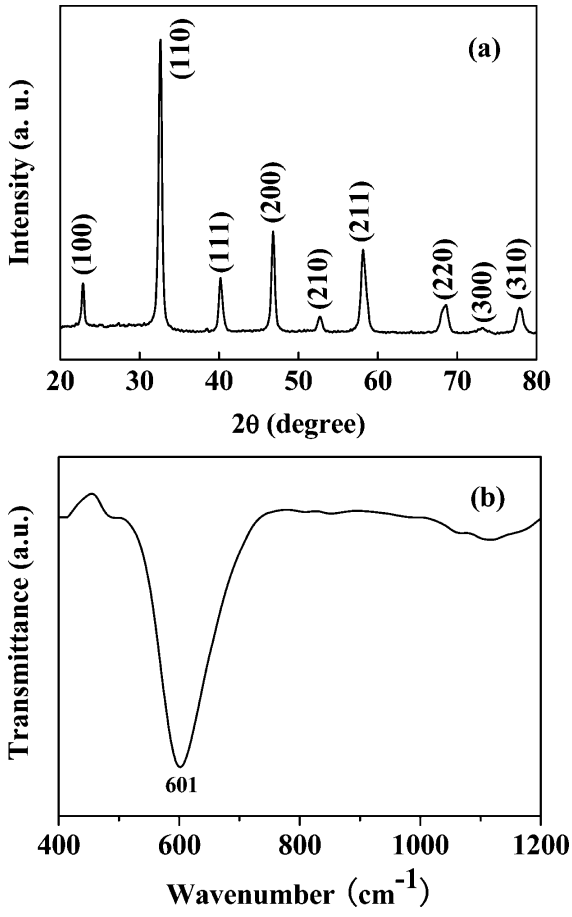

FIGURE 2. (a) XRD pattern of $LaMnO_{3+\delta}$ nanofibers. (b) FT-IR powder absorption spectra of $LaMnO_{3+\delta}$ samples.

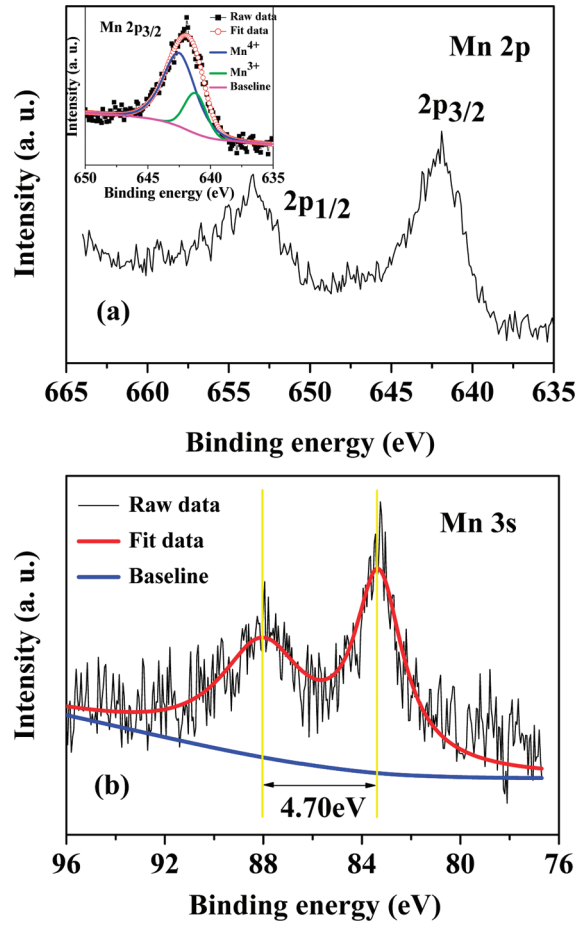

FIGURE 3. (a) Mn 2p core level XP spectrum of $LaMnO_{3+\delta}$ nanofibers. Inset: Peak fitting on the Mn $2p_{3/2}$ peak using the XPSPEAK software. (b) The Mn 3s core level XP spectrum of $LaMnO_{3+\delta}$ samples.

etry due to the electric neutrality, and the formula should be written as $LaMnO_{3+\delta}$ (21).

The zero-field-cooled (ZFC) and field-cooled (FC) magnetization curves recorded in a magnetic field of 100 Oe between 4 and 350 K are shown in Figure 4a. The results show that the fibers are ferromagnetic at low temperature, which attribute to the high Mn^{4+} content of the samples and small size effect. The T_c of the fibers, which was determined as the minimum of the derivative of the magnetization, $dM_{FC}(T)/dT$, is approximately 255 K. The appearance of ZFC curve is general characteristics of magnetic nanoscale systems. When the grain is ferromagnetic and sufficiently small, it is not energetically favorable to the bulk ferromagnetism. The magnetic anisotropy of the ferromagnetic grain generates potential barriers, which at low temperature prevent the magnetization vector from rotating to the direction of minimum energy in the applied magnetic field. Therefore, the ferromagnetic grain is blocked and the temperature is called "blocking temperature" T_B (22), and in the magnetic measurement, the ZFC curve show a maximum at the T_B. According to the core−shell scenario of nanometric grains, for comparatively larger size grains, $T_B \approx T_c$ because of the dominance of core magnetic exchange energy and because of the ineffectiveness of thermal energy. For comparatively smaller size grains, where mainly core exchange as well as anisotropy energy are very weak, and thermal energy can dominate over those two, $T_B \ll T_c$ and the sample show superparamagnetic property when the temperature is above the T_B and below T_c (23). In our case, the result of magnetization curves shows that the T_c onset of the fibers is approximately 310 K, and the T_B is about 180 K. The $M(H)$ hysteresis loops of the $LaMnO_{3+\delta}$ samples at different temperatures from T=5 to 300 K in the magnetic field range of −30 to 0 to +30 kOe is shown as Figure 4b. The results shows the sample shows ferromagnetic property below T_B and weak ferromagnetic property above the T_B and below T_c. The grain size determines the magnetic property. For the size of about 5 nm, the blocking temperature is about 93 K and far below the T_c (about 230 K), and the sample show superparamagnetic property (24). In this study, the average grain size of our fibers is about 20 nm, the T_B is below but not far below the T_c. It is the intermediate case between these two mentioned above, because the grain size is the critical point of nanoscale effect. The mainly core exchange as well as anisotropy energy are weak but not weak enough to make thermal energy dominate over those two above the T_B, so our sample shows weak ferromagnetic property above the T_B and below T_c (180 and 220 K) and superparamagnetic property near the T_c onset (280 K). Upon the sample being cooled in a magnetic field (100 Oe), the nanograins become trapped in the higher-magnetized state and thermal energy is not required to pass over the potential barriers to return to their

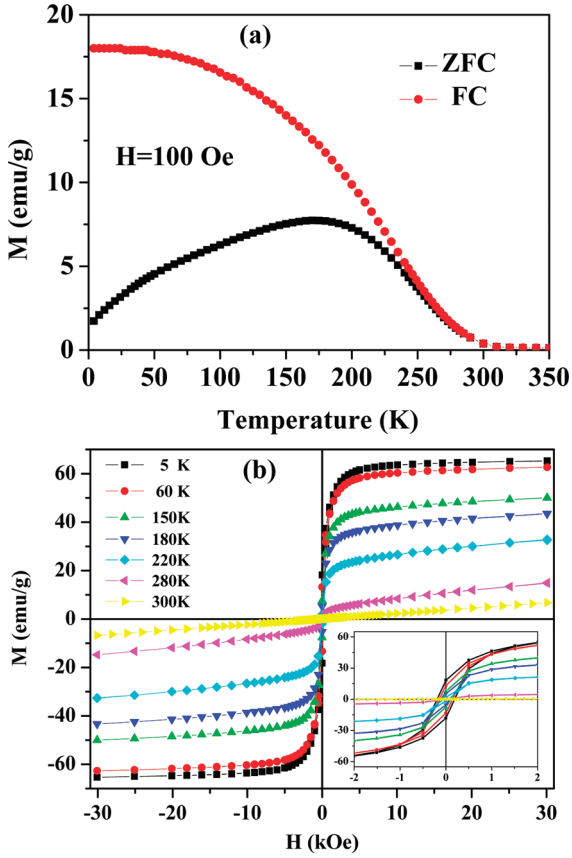

FIGURE 4. (a) Temperature dependence of ZFC and FC magnetization of the $LaMnO_{3+\delta}$ Nanofibers, recorded in $H = 100$ Oe. (b) $M(H)$ hysteresis loops of the $LaMnO_{3+\delta}$ samples at different temperatures from $T = 5$ to 300 K in the magnetic field range of −30 to 0 to +30 kOe. The inset shows the same plots at a narrow range of magnetic field of −2 to 0 to +2 kOe.

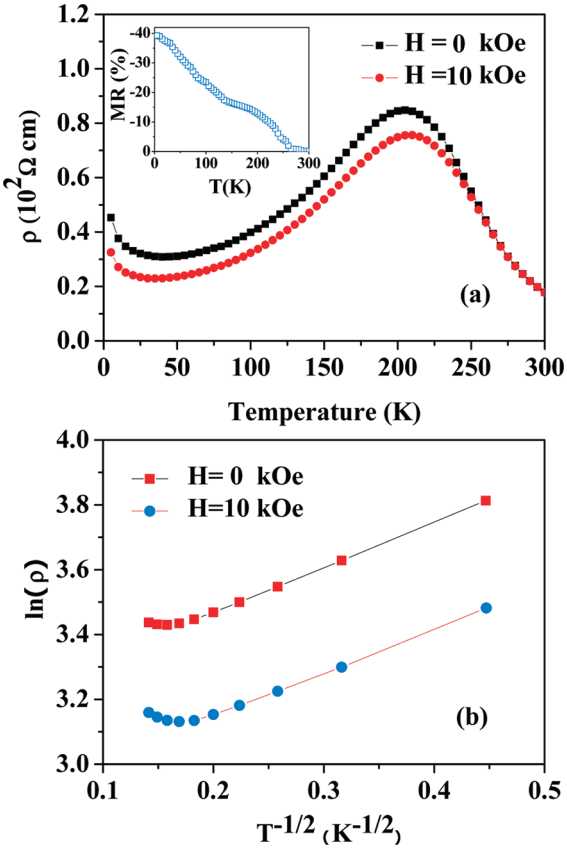

FIGURE 5. (a) Temperature dependence of the electrical resistivity of the $LaMnO_{3+\delta}$ Nanofibers at $H = 0$ and 10 kOe. Inset: temperature dependence of magnetoresistance in an applied magnetic field of 10 kOe. (b) Dependence of ln(ρ) versus $T^{-1/2}$ curves below 45 K.

lower-magnetized equilibrium configuration (25). Therefore, there is no decrease in the FC curve below the T_B.

Figure 5a shows the samples resistivity, recorded under $H = 0$ and 10 kOe, as a function of the temperature. The results show that there is a clear insulator-to-metal transition around $T_{max} \approx 210$ K, quasi-metallic ($dR/dT > 0$) behavior in a wide temperature range 50 K < T < 210 K and a sharp upturn of resistivity at low temperature below $T \approx 45$ K. Resistivity curves of $H = 0$ and 10 kOe measurements start to diverge at $T < 285$ K, and the negative magnetoresistance $MR_H = [(\rho(H) - \rho(0))/\rho(H)] \times 100\%$ increases monotonically with decreasing temperature, reach to the maximum 39.3% at 5 K, see the inset to Figure 5a. The resistivity exhibit a rapid upturn below a temperature of about 45 K, indicating insulating characteristics at lower temperature, similar to the previous reports on various polycrystalline manganites and nanoparticles of manganites (2, 5, 6). The upturn of the low-temperature resistivity may originate from the Coulomb blockade (CB) phenomenon because of the presence of insulating tunneling barriers in the system. Balcells et al. suggested theoretical expression describing the conductivity of granular materials and attributed the experimentally observed behavior of the resistivity to the effects of the CB effect and insulating tunneling barriers in nanograins (26). According to the model, the resistivity of a granular metal obeys the relation $\rho = A\exp[(\Delta/T)^{1/2}]$, where Δ is proportional to the charging energy $E_c = e^2/(4\pi\varepsilon_0)F(s/d)$. E_c is the energy required to create a positive-negative charged pair of grains, ε_0 is the vacuum permittivity, and the function $F(s/d)$ depends on the shape of a granule. Parameters s and d are the grain size and separation between grains, respectively. The ln(ρ) versus $T^{-1/2}$ curves in the Figure 5b show linear in the temperature range of 10−45 K. After fitting, we can obtain that the value of Δ is 1.90 and 1.74 K at zero field and 10 kOe, respectively, which is much lower than the reported nanoparticles values (e.g., the value of Δ is 14.2 and 12.1 K at zero field and 14 kOe in ref 5, respectively; 5.48 and 7.75 K at zero field and 50 kOe in the ref 6, respectively). Because $LaMnO_{3+\delta}$ nano grains are close-packed in the nanofibers, the charging energy of our samples is lower than that of normal nanoparticles. Therefore, the Δ of our fibers is much lower than that of the $LaMnO_{3+\delta}$ nanoparticles and the corresponding resistivity decreases 2 orders of magnitude (5, 6).

In summary, $LaMnO_{3+\delta}$ nanofibers have been prepared by a sol−gel process and electrospinning technique, in which nearly 70% of Mn atoms are Mn^{4+}. The average particle size of our fibers is approximately 20 nm, which is the critical size producing the nanoscale effect. The nanofibers exhibit a very broad magnetic transition with $T_c \approx 255$ K, and start to show the ferromagnetism around 310 K. The blocking temperature T_B is about 180 K. The sample shows weak ferromagnetic property above the T_B and below T_c and super-

paramagnetic property near the T_c onset. The resistivity measurement show a metal−insulator transition near 210 K and an upturn at about 45 K, which is interpreted in terms of the CB effect. The charging energy and resistivity are much lower than that of the normal $LaMnO_{3+\delta}$ nanoparticles.

Acknowledgment. We thank Prof. Xudong Zhao of Jilin University (China) for his helpful discussion. This work was financially supported by the National Science Foundation of China (Grants 20831004, 20921002, and 21071141).

Note Added after ASAP Publication. This paper was published on the Web on September 15, 2010, with minor errors in Figure 5a. The corrected version was reposted on September 21, 2010.

REFERENCES AND NOTES

(1) Zhou, J. S.; Goodenough, J. B. *Phys. Rev. Lett.* **2006**, *96*, 247202.
(2) Xu, Y.; Zhang, J. C.; Cao, G. X.; Jing, C.; Cao, S. X. *Phys. Rev. B* **2006**, *73*, 224410.
(3) Niebieskikwiat, D.; Salamon, M. B. *Phys. Rev. B* **2005**, *72*, 174422.
(4) Zener, C. *Phys. Rev.* **1951**, *81*, 440–444.
(5) Markovich, V.; Jung, G.; Fita, I.; Mogilyansky, D.; Wu, X.; Wisniewski, A.; Puzniak, R.; Froumin, N.; Titelman, L.; Vradman, L.; Herskowitz, M.; Gorodetsky, G. *J. Phys. D: Appl. Phys.* **2008**, *41*, 185001.
(6) Wang, X. L.; Li, D.; Shi, C. X.; Li, B.; Cui, T. Y.; Zhang, Z. D. *Physica B* **2010**, *405*, 1362–1368.
(7) Markovich, V.; Fita, I.; Mogilyansky, D.; Wisniewski, A.; Puzniak, R.; Titelman, L.; Herskowitz, M.; Gorodetsky, G. *J. Phys.: Condens. Matter* **2007**, *19*, 346210.
(8) Wang, Z. L. *Annu. Rev. Phys. Chem.* **2004**, *55*, 159–196.
(9) Li, D.; Xia, Y. N. *Adv. Mater.* **2004**, *16*, 1151–1170.
(10) Shao, C. L.; Kim, H. Y.; Gong, J.; Lee, D. K. *Nanotechnology* **2002**, *13*, 635–657.
(11) Le, V.; Reddy, M.; Jose, R.; Chowdari, B.; Ramakrishna, S. *J. Phys. Chem. C* **2010**, *114*, 664–671.
(12) Hosono, E.; Wang, Y. G.; Kida, N.; Enomoto, M.; Kojima, N.; Okubo, M.; Matsuda, H.; Saito, Y.; Kudo, T.; Honma, I.; Zhou, H. S. *ACS Appl. Mater. Interfaces* **2010**, *2*, 212–218.
(13) Wang, Z. L.; Liu, X. J.; Lv, M. F.; Chai, P.; Liu, Y.; Zhou, X. F.; Meng, J. *J. Phys. Chem. C* **2008**, *112*, 15171–15175.
(14) Dezanneau, G.; Audier, M.; Vincent, H.; Meneghini, C.; Djurado, E. *Phys. Rev. B* **2004**, *69*, 014412.
(15) Zhou, X. F.; Zhao, Y.; Cao, X. Y.; Xue, Y. F.; Xu, D. P.; Jiang, L.; Su, W. H. *Mater. Lett.* **2008**, *62*, 470–472.
(16) Wang, J. X.; Zheng, X. Q.; Dong, X. T.; Qu, Z.; Liu, G. X. *Appl. Phys. Res.* **2009**, *1*, 30–36.
(17) Li, K. B.; Li, X. J.; Zhu, K. G.; Zhu, J. S.; Zhang, Y. H. *J. Appl. Phys.* **1997**, *81*, 6943–6947.
(18) Julien, C. M.; Massot, M.; Poinsignon, C. *Spectrochim. Acta A* **2004**, *60*, 689–700.
(19) Beyreuther, E.; Grafström, S.; Eng, L. M.; Thiele, C.; Dörr, K. *Phys. Rev. B* **2006**, *73*, 155425.
(20) Galakhov, V. R.; Demeter, M.; Bartkowski, S.; Neumann, M.; Ovechkina, N. A.; Kurmaev, E. Z.; Lobachevskaya, N. I.; Mukovskii, Y. M.; Mitchell, J.; Ederer, D. L. *Phys. Rev. B* **2002**, *65*, 113102.
(21) Töpfer, J.; Goodenough, J. B. *J. Solid State Chem.* **1997**, *130*, 117–128.
(22) Lin, Y. C. *Mater. Sci. Eng., B* **2000**, *77*, 40–49.
(23) Dey, P.; Nath, T. K. *Phys. Rev. B* **2006**, *73*, 214425.
(24) Zhang, T.; Li, X. G.; Wang, X. P.; Fang, Q. F.; Dressel, M. *Eur. Phys. J. B* **2010**, *74*, 309–312.
(25) Hickey, B. J.; Howson, M. A.; Musa, S. O.; Tomka, G. J.; Rainford, B. D.; Wiser, N. *J. Magn. Magn. Mater.* **1995**, *147*, 253–259.
(26) Balcells, L.; Fontcuberta, J.; Martinez, B.; Obradors, X. *Phys. Rev. B* **1998**, *58*, 14697–14700.

AM1004738

LETTER